An X-ray investigation of the NGC 346 field in the SMC (3): *XMM-Newton* data

Yaël Nazé[1] and Jean Manfroid[2,3]

Institut d'Astrophysique et de Géophysique, Université de Liège, Allée du 6 Août 17, Bat. B5c, B4000 - Liège (Belgium)

naze@astro.ulg.ac.be, manfroid@astro.ulg.ac.be

Michael F. Corcoran

Universities Space Research Association, 7501 Forbes Blvd, Ste 206, Seabrook, MD 20706, and Laboratory for High Energy Astrophysics, Goddard Space Flight Center, Greenbelt, MD 20771 (USA)

corcoran@barnegat.gsfc.nasa.gov

Ian R. Stevens

School of Physics & Astronomy, University of Birmingham, Edgbaston, Birmingham B15 2TT (UK)

irs@star.sr.bham.ac.uk

ABSTRACT

We present new *XMM-Newton* results on the field around the NGC 346 star cluster in the SMC. This continues and extends previously published work on *Chandra* observations of the same field. The two *XMM-Newton* observations were obtained, respectively, six months before and six months after the previously published *Chandra* data. Of the 51 X-ray sources detected with *XMM-Newton*, 29 were already detected with *Chandra*. Comparing the properties of these X-ray sources in each of our three datasets has enabled us to investigate their variability on times scales of a year. Changes in the flux levels and/or spectral properties

---

[1]Research Fellow F.N.R.S.

[2]Research Director F.N.R.S.

[3]Visiting Astronomer, European Southern Observatory

were observed for 21 of these sources. In addition, we discovered long-term variations in the X-ray properties of the peculiar system HD 5980, a luminous blue variable star, that is likely to be a colliding wind binary system, which displays the largest luminosity during the first *XMM-Newton* observation.

Subject headings: (galaxies:) Magellanic Clouds – X-rays: individual (NGC 346) – X-rays: galaxies: clusters – stars: individual (HD 5980)

1. Introduction

The giant H II region N66 of the Small Magellanic Cloud (SMC) is the largest star formation region of that galaxy. It notably harbors NGC 346, a young cluster containing a wealth of massive stars, and HD 5980, a peculiar system that underwent a LBV-type eruption at the end of the last century. *ROSAT* and *ASCA* observations have also revealed the presence of a few X-ray binaries (XRBs) in this field (see e.g. Haberl & Sasaki 2000; Tsujimoto et al. 1999), some of which were later found to harbor pulsars (for a review, see Haberl & Pietsch 2004).

Recently, a new generation of powerful X-ray observatories has been launched and the XMEGA[1] consortium used this opportunity to observe the X-ray emission from the NGC 346 field in greater detail. The results of a 100 ks *Chandra* observation have been given in two previous articles. In Nazé et al. (2003a, hereafter Paper I), we reported the first detections in the X-ray domain of the cluster and HD 5980. The X-ray emission from NGC 346 appeared tightly correlated with the cluster's core, while that of HD 5980 was found to be bright and variable on the short timescale. In Nazé et al. (2003b, hereafter Paper II), we analyzed the X-ray properties of the 75 point sources discovered in the field, and found possible counterparts to 32 of these sources. We refer the reader to these papers for detailed results and a thorough introduction to the importance of the NGC 346 field. This third Paper of the series is meant to supplement the two previous ones. Here, we continue our investigation of the field with the analysis of two *XMM-Newton* datasets, which provide a wider field compared to the *Chandra* data and allow us to examine the issue of source variability on timescales of seconds to months.

The observations and data reduction are presented in §2. Next, the properties of the sources detected by *XMM-Newton* are discussed in §3, where they are also compared to

[1]http://lheawww.gsfc.nasa.gov/users/corcoran/xmega/xmega.html

previous data available. In §4, we focus the discussion on HD 5980, the supernova remnant SNR 0056−72.5, and the XRBs. We conclude in §5.

2. Observations

NGC 346 was observed once with the *Chandra* Observatory and twice with the *XMM-Newton* satellite. The *Chandra* data, taken on 2001 May 15-16 for 100 ks, have been extensively analyzed in Papers I and II, and we will focus here only on the *XMM-Newton* data. The first *XMM-Newton* observation took place during revolution 0157, on Oct. 17 2000 for about 20 ks. It is a public dataset part of the *XMM-Newton* Science Archive. The second observation, of length ∼30 ks, was obtained by our XMEGA group during revolution 0357, on Nov. 20-21 2001. The EPIC MOS cameras (Turner et al. 2001) were used in full frame mode during both revolutions, while the EPIC pn camera (Strüder et al. 2001) was used in full frame mode during Rev. 0357 and in extended full frame mode during Rev. 0157. For both observations, a medium filter was added to reject optical light.

We used the Science Analysis Software (SAS) version 5.4.1. (Jansen et al. 2001) to reduce the EPIC data. These data were first processed through the pipeline chains, and then filtered. For EPIC MOS, only events with a pattern between 0 and 12 and passing through the #XMMEA_EM filter (i.e. flag&0x766b000=0) were considered. For EPIC pn, we kept events with flag=0 and a pattern between 0 and 4. The resulting exposure times were 19.6 ks (EPIC MOS) and 15.5 ks (EPIC pn) for Rev. 0157, and 26.7 ks (EPIC MOS) and 21.7 ks (EPIC pn) for Rev. 0357.

To search for contamination by low energy protons, we have further examined the light curve at high energies (PI>10000, ∼E>10 keV, and with pattern=0). Throughout both observations, a rather large high energy count rate (on average, 0.25 cts s^{-1} for EPIC MOS and 1.25 cts s^{-1} for EPIC pn) was detected but since no clear flare is present, we decided to keep the whole exposure in both cases. Further analysis was performed using the SAS version 5.4.1. and the FTOOLS tasks (Blackburn 1995). The spectra were analyzed and fitted within XSPEC v11.0.1 (Arnaud 1996).

3. Source Properties

The combined EPIC images of the NGC 346 field of both *XMM-Newton* datasets are shown in Fig. 1. Several point sources can be spotted throughout the field and some of them are clearly seen to vary between the two observations. To create a catalog of these discrete

X-ray sources, we applied for each observation the SAS detection meta-task *edetect_chain* simultaneously to the data from all three EPIC cameras. Due to the rather high background during these observations, we decided to restrict the energy range to 0.4−4.0 keV, and then created images in the following three energy bands for input in *edetect_chain*: S=0.4−1.0 keV, M=1.0−2.0 keV and H=2.0−4.0 keV. We eliminated false detections due to structures in the extended emission near HD 5980, gaps, or remaining bad pixels and bad columns. We also rejected sources with a small detection likelihood (i.e. with a logarithmic likelihood in one detector $\ln p_i \ll 5$ and/or a combined likelihood for the three detectors $\ln p_i < 30$). We have compared the lists found in each case and finally constructed a definitive list of 51 sources[2] which are presented in Table 1 by increasing Right Ascension (RA). Note that 29 of these were already detected in our *Chandra* observation: for these sources, we will use the *Chandra* source number from Paper II, which will be quoted as [NHS03] # throughout this paper, whereas for the sources specific to the *XMM-Newton* observations, we will use a letter as identifier. Most of the undetected *Chandra* sources have an ACIS-I count rate smaller than 8×10^{-4} cts s^{-1} (see also §3.3). This is not surprising since the smallest *XMM-Newton* count rates detected in our observations are about 10^{-3} cts s^{-1} for EPIC MOS and 2×10^{-3} cts s^{-1} for EPIC pn. This detection threshold is roughly an order of magnitude larger than for *Chandra* (10^{-4} cts s^{-1}). The smaller exposure time, combined with the loss of resolution due to the larger Point Spread Function (PSF) of *XMM-Newton* and a rather high background explain why we detect only one third of the *Chandra* sources.

The count rates of the sources in each instrument are also presented in Table 1. A missing count rate indicates a source (at least partly) in gaps or out of the field-of-view (FOV) for the instrument considered. If the task *edetect_chain* provides vignetting- and background-corrected count rates, an additional correction is needed. Following the User Support Group, it actually appears that the SAS task *eexpmap*, used by the meta-task *edetect_chain*, does not consider all the necessary exposure information. In particular, it neglects out-of-time (OOT) and deadtime corrections. If this is negligible for the EPIC MOS data, not correcting for OOT events in the EPIC pn data implies an overestimation of the exposure time (and

---

[2]The *XMM-Newton* data from Rev. 0157 were used in the creation of the 1XMM catalog (XMM-SSC 2003), which was released recently. However, this catalog does not seem very accurate in this field, probably as a result of the difficulties of the automated source detection algorithms in complicated fields like this one (see also Claeskens et al. 2004). The 1XMM source list may have been created using a very low detection threshold or maybe its algorithm was somewhat confused by the presence of extended emissions: most of the 108 1XMM sources in the field simply do not appear in the combined EPIC images. If we restrict ourselves to the sources securely detected in the three cameras (i.e. with $Qflag = 4$), only 20 sources remain, but some obvious, bright X-ray sources are not part of this restricted list and in addition, some of the "secure detections" are actually the same source detected twice. A good source list for this field thus still needed to be made.

thus an underestimation of the count rates) by 6.3% for the full frame mode (Rev. 0357) and 2.3% for extended full frame mode (Rev. 0157). We thus have corrected the pn count-rates provided by *edetect_chain* by this amount, and the result is shown in Table 1. The presented hardness ratios HR1 and HR2 have been calculated for the pn data as (M−S)/(M+S) and (H−M)/(H+M), respectively. The last column of Table 1 yields information on the nature of the X-ray source (e.g. Haberl & Pietsch 2004) or of its counterpart (Paper II and Table 3).

In addition to these point sources and the supernova remnant (SNR) near HD 5980, we note the possible presence of extended emission north of source E and near position $0^h58^m25^s$ $-72°00'40''$, but their low surface brightness did not permit to derive any precise physical information on these sources.

3.1. Source spectra and luminosities

For the 12 brightest sources, we extracted the sources' spectra in circles of minimum radius 25″, and chose annuli surrounding the sources or nearby circles for background subtraction. Using the SAS's *rmfgen* and *arfgen* tools we then generated the response matrix file and ancillary reponse file, necessary to any spectral analysis. The spectra were finally binned to obtain at least 10 cts per bin, and were then analyzed within XSPEC. Bins with energies below 0.4 keV or above 10.0 keV were discarded. Since their signal-to-noise was generally rather low, the spectra were fitted with simple models, i.e. an absorbed power-law or an absorbed *mekal* model. As fits to the MOS and pn spectra generally gave similar results, within the errors, we chose to fit simultaneously all EPIC data available for a particular observation to get the smallest errors. The results of these fits are presented in Table 2, but note that *mekal* models (Kaastra 1992) with unconstrained and unrealistically high temperatures (i.e. $kT > 10.0$ keV) were not included in that table. We caution that the abundance specific to the SMC, $Z = 0.1\,Z_\odot$, was used only for the *mekal* models, not for the absorbing column (like e.g. in Haberl & Pietsch 2004). Absorbing columns larger than $\sim 4 \times 10^{20}$ cm^{-2} indicate absorption within the SMC over and above the Galactic column. In such case the metallicity of the absorbing material may be low, and a good estimate of the SMC absorbing column can be easily derived by multiplying the excess column by a factor 10.

The spectral properties of eight of our sources were also determined by two other teams (Sasaki, Pietsch, & Haberl 2003; Majid, Lamb, & Macomb 2004). The properties derived here are generally in good agreement with their values, since the confidence intervals overlap for all sources except [NHS03] 75. In this last case, the spectral changes might actually be

real, since the source is a varying X-ray binary (see §§3.3.2 and 4.3).

3.2. Counterparts

For the 29 *XMM-Newton* sources in common with *Chandra* data, we refer the reader to the extensive discussion of Paper II, which we will not repeat here. To search for optical counterparts to the remaining X-ray sources, we have followed a procedure similar to that of Paper II. We have first cross-correlated the source list with the public databases (USNO B1.0, GSC 2.2, 2MASS All Sky Survey) and then with our Wide Field Imager (WFI) data. Before correlating our source list with these optical databases, we have determined the mean shifts between *Chandra* and each *XMM-Newton* observation. Since there exists a shift of $+1\farcs6$ in RA and $-1\farcs2$ in DEC between actual world coordinates and *Chandra*'s (see Paper II), we applied a shift of +0.26s in RA to coordinates of Rev. 0357 and $+2''$ in DEC for Rev. 0157. All objects within $5''$ - the PSF width of *XMM-Newton* - of the X-ray sources were considered as possible counterparts and are listed in Table 3. Fig. 2 presents a color-magnitude diagram similar to Fig. 6 of Paper II. The majority of the sources are within the main sequence of NGC 346 but we note that the counterparts of sources I & N appear as slightly evolved early-type stars and that a few counterparts (A,B,Q) apparently belong to a second population of the SMC, that is not physically associated with the NGC 346 cluster itself.

We have also compared our source list to the *ROSAT* and *ASCA* catalogs of SMC X-ray sources (Kahabka et al. 1999; Haberl et al. 2000, hereafter [HFP2000]; Sasaki, Haberl, & Pietsch 2000, hereafter [SHP2000]; Yokogawa et al. 2000, hereafter [YIT2000]). Thirteen of the 22 *XMM-Newton* sources were previously detected and we noted in Table 3 their *ROSAT* or *ASCA* identification.

3.3. Source Variability

3.3.1. Short-Term Variability

We have also analyzed the lightcurves of these 12 brightest sources. Using the same regions as in §3.1, we created lightcurves for each source and associated background region. The sources' lightcurves were then background-subtracted, corrected for good time intervals, and analyzed within our own software. Using Kolmogorov-Smirnov, χ^2, and modified probability of variability (see Sana et al. 2004) tests, we found no source significantly variable in all three EPIC camera during a single observation.

3.3.2. Long-Term Variability

In Paper I and II, we have extensively analyzed the sources detected by *Chandra*. Among other properties, we have determined the detailed spectral characteristics of 15 ACIS-I sources. Four out of these 15 sources were bright enough to provide a valuable EPIC spectra that can be compared with our previous results (see Paper II and Table 2). All EPIC spectra present a lower absorption column, compared to *Chandra*'s. This systematic difference could most probably be attributed to calibration problems at low energies, since the calibrations of both satellites are still ongoing (in particular to the recently discovered degradation of the ACIS quantum efficiency). In addition, these sources also present a clearly variable X-ray luminosity over the three observations:

- [NHS03] 4 has approximately the same flux in the *Chandra* data than in the *XMM-Newton* data of Rev. 0157, but it increased by 70% in the last *XMM-Newton* observation.
- [NHS03] 6 presents similar characteristics in the *Chandra* data and the first *XMM-Newton* observation, but the power law steepens and the flux has dramatically decreased by a factor of $\sim$25 in the last *XMM-Newton* observation.
- [NHS03] 60 has a flux reduced by at least a factor 3 in the *Chandra* observation, compared to the *XMM-Newton* ones. With its rather large absorbing column and large power law energy slope Γ, it is considered in Sasaki, Pietsch, & Haberl (2003) as a possible AGN candidate.
- [NHS03] 69 presents only a small increase of flux ($\sim$20%) in the last *XMM-Newton* observation, and marginal variations of the power law's exponent.

The spectral characteristics of ten additional *Chandra* sources are known, but they present too few counts in the *XMM-Newton* observations to give any meaningful spectrum. To detect possible variations for these sources, we used the spectral information from Paper II and PIMMS[3] to predict the *XMM-Newton* EPIC count rates, which we have then compared directly to the observed ones, since the output of the task *edetect_chain* is an equivalent on-axis count rate. By this procedure, we detected no flux variation for [NHS03] 1, 19, 20, 29, 30, and 70, but four additional varying sources were also found:

---

[3]Available at http://heasarc.gsfc.nasa.gov/Tools/w3pimms.html. Note that the closest kT and $Z = 0.2Z_{\odot}$ (the lowest available) were used for the mekal models.

- Using the *Chandra* data, we expect [NHS03] 10 and 71 to be brighter by 40% (EPIC MOS) and 200% (EPIC pn) for the former, and 10% (EPIC MOS) and 50% (EPIC pn) for the latter.

- The expected EPIC pn count rate of [NHS03] 24 is a factor $\sim$4 larger than the value observed at Rev. 0157. However, this cannot be confirmed by the EPIC MOS data of Rev. 0157, since the source falls in a detector gap at that time.

- [NHS03] 46 possesses an *XMM-Newton* count rate double of what is expected on basis of the *Chandra* data.

We also note that the *Chandra* sources [NHS03] 23, 37, 47, and 61 are detected with *XMM-Newton* although they possessed an ACIS-I count rate smaller than 8×10^{-4} cts s^{-1}, i.e. so small that it should have prevented their detection by *XMM-Newton*. On the contrary, [NHS03] 45 and 49 remain undetected (with *XMM-Newton* count rates $< 1.5 \times 10^{-3}$ cts s^{-1} for EPIC MOS and $< 3 \times 10^{-3}$ cts s^{-1} for EPIC pn) whereas they were expected to show up on the basis of their relatively large *Chandra* count rate (9.8 and 11.0 $\times 10^{-4}$ cts s^{-1}, respectively). These six sources may be added to the list of variable X-ray sources.

In addition, for the sources out of *Chandra* ACIS-I FOV, we can compare directly the count rates and/or spectral properties between both *XMM-Newton* observations and we found 7 additional varying sources:

- [NHS03] 75 has undergone a dramatic increase of luminosity by a factor $\sim$23 in the last *XMM-Newton* observation. As for [NHS03] 6, the power law steepened when the flux was lowest (see Fig. 3).

- Source G has a slightly lower flux (a 15% decrease) in the last *XMM-Newton* observation and the flux of Source I is larger by 60% in the first *XMM-Newton* observation. Regarding the nature of these sources, we may note that with its large absorbing column and Γ, Source G is a good AGN candidate, whereas Source I possesses a bright blue counterpart indicating a possible X-ray binary nature (see §4.3 for more details).

- Source L has exhibited a luminosity decreased by 75% in the data from Rev. 0157.

- The count rate of Source M has increased by 75% in the last *XMM-Newton* observation.

- Source S has experienced an increase of 50% in the power law exponent, associated with a decrease of the flux by a factor of 2 in the last *XMM-Newton* observation. This variation is similar to the behavior exhibited by [NHS03] 6 and 75.

- The flux of Source V has doubled in the last *XMM-Newton* observation.

There were also some 13 sources detected only in one of the two *XMM-Newton* observations. However, most of these sources possess a very low count rate, close to the detection limit ($\sim 10^{-3}$ cts s^{-1}). Their absence could well be explained by a simple statistical fluctuation, and the upper limits derived in the observation where they are missing are compatible with a constant count rate (see Table 1). By comparing the observed count rates in one dataset to the upper limits calculated for the other *XMM-Newton* observation, we nevertheles inferred count rate variations for Source N, of at least 20% in EPIC MOS, and at least 170% for EPIC pn. In addition, a large luminosity decrease is detected for source D. This source is at best marginally detected in the *XMM-Newton* data of Rev. 0357, while it is one of the brightest sources in the *XMM-Newton* observation made at Rev. 0157: the count rate of this source changes by a factor of at least 25 between our two *XMM-Newton* observations. In addition of finding pulses of period 280.4s, Tsujimoto et al. (1999) already discovered dramatic flux variations for this source by comparing *ROSAT* and *ASCA* observations, making Source D one of the most interesting X-ray binaries of this field.

Comparing with older X-ray catalogs, we also note that the *ROSAT* sources [HFP2000] 103, 173, 185, 186, 207 and [KPF99] 157 are missing in the *XMM-Newton* observation. Since these six *ROSAT* sources were not particularly faint *ROSAT* sources, their non-detection suggests a strongly variable nature. Using the SAS task *esensmap* for a likelihood of 10, we derived upper limits on the *XMM-Newton* count rate of these sources of $1.5-2.5\times10^{-3}$ cts s^{-1} for EPIC MOS and $3-4\times10^{-3}$ cts s^{-1} for EPIC pn. We note however that [HFP2000] 186 was already undetected in the *Chandra* observation (see Paper II), i.e. its ACIS-I count rate was lower than 10^{-4} cts s^{-1}. In addition, the ACIS-I count rates of the *ROSAT* sources [HFP2000] 173 and 185 (=[NHS03] 11 and 16 in Paper II) were very low, about 2×10^{-4} cts s^{-1}, in our *Chandra* data. If these three sources did not change since then, they are well below the detection threshold of our *XMM-Newton* observations.

4. Comments on individual sources

4.1. HD 5980

We reported the first detection of HD 5980 at X-ray energies in Paper I. But this peculiar star was also observed twice by *XMM-Newton* and in fact, the *XMM-Newton* data of Rev. 0157, which were taken before the *Chandra* observation, constitute the first actual detection of HD 5980 in X-rays. When *Chandra* caught the system at orbital phase $\phi = 0.23 - 0.30$ (using the ephemeris of Sterken & Breysacher 1997), the first *XMM-Newton* observation

sampled phase $\phi = 0.36 - 0.38$ (eclipse of star A, the eruptor, by star B), while the data taken during Rev. 0357 show HD 5980 at $\phi = 0.09 - 0.11$ (periastron). However, the poorer resolution of *XMM-Newton* compared to *Chandra*'s renders difficult the disentangling of the source from the surrounding SNR (see Fig. 4), especially since the flux and spectral properties of this SNR change spatially (see Paper I).

To overcome these problems and provide hints of the intrinsic variations of the star, we chose three circular regions of 15″ radius, which we will called 'hd', 'snr', and 'bkgd'. Region 'hd' is centered on HD 5980, but also sampled part of the SNR. Region 'snr' is close-by area containing only contributions from the SNR. It is centered on *Chandra* coordinates $0^h59^m32.5^s$ $-72°10'26''$. Region 'bkgd' is a nearby background region situated at *Chandra* coordinates $0^h59^m45^s$ $-72°11'00''$. To eliminate the large background and sensitivity variations that may exist between our observations, we computed the ratio (hd−bkgd)/(snr−bkgd) in four energy ranges for each observation and for each instrument. We present in Fig. 5 the evolution with phase of that ratio for the ranges 0.4−1.0 keV, 1.0−2.0 keV and 0.4−10.0 keV. Note that the results from the last chosen energy range, 2.0−4.0 keV, are too noisy and thus not very reliable: they are not displayed in Fig. 5. There is no significant change between the *XMM-Newton* data from Rev. 0357 and the *Chandra* observation, but the X-ray luminosity of HD 5980 has clearly increased during the first *XMM-Newton* observation. This variation is particularly well seen in the harder range, which is not surprising since the emission from the SNR dominates at low energies.

The intrinsic X-ray emission of a colliding-wind system like HD 5980 is expected to vary as $1/D$ (D being the separation between the components) and it should thus be larger at periastron. We do not observe such a variation, but the effects of a varying absorption column might explain the observed changes. However, we may note that HD 5980 is known to present secular variations in the optical domain: with only three observations, it is not yet possible to disentangle the possible long-term variations of the X-ray luminosity (for example related to the 1994 eruption) from systematic changes linked to the orbital motion. Note that a more complete discussion about HD 5980 variations will be presented by Flores et al. (in preparation), but we also note that monitoring of HD 5980 with the *Chandra* satellite (the only one easily capable of disentangling HD 5980 from the SNR) would be of utmost interest to better constrain the system's physical characteristics.

4.2. SNR 0056−72.5

Apart from the SNR surrounding HD 5980, a second supernova remnant is present in the *XMM-Newton* FOV: source E. As could be expected from such an object, this source

did not vary between both *XMM-Newton* observations. It is correlated with an extended non-thermal radio source discovered by Ye, Turtle, & Kennicutt (1991). This radio source has a size of 100″×80″ (or 160″×160″ if we use the lower contours of Ye et al.). The X-ray source corresponds exactly with the peak of the radio source and we may note that, as far as the *XMM-Newton* resolution can conclude, the *XMM-Newton* source is point-like, i.e. not extended as in the radio range. However, its X-ray luminosity ($\sim 9 \times 10^{34}$ erg s^{-1}) is quite large for a putative isolated neutron star born in the supernova event (Haberl 2003). The source also presents a rather hard spectra, that was well fitted by a power-law of energy slope $\Gamma \sim 1.7$ but not by a thermal model (kT of 4 to 50 keV). Finally, some faint extended emission may also be present to the north of the X-ray source, and it correlates well with an extension of the source at radio wavelengths.

4.3. X-ray Binaries

Six X-ray binary candidates were proposed in our *XMM-Newton* FOV by Haberl & Sasaki (2000): [NHS03] 4, 6 & 70; and Sources D, S & V. Their status as XRBs is now confirmed by a large body of evidences. The X-ray sources [NHS03] 6 & 70, and D & S were found to pulsate (Tsujimoto et al. 1999; Sasaki, Pietsch, & Haberl 2003; Macomb et al. 2003)[4]. All sources have also been found to vary on short- or long- timescales in *ROSAT*, *Chandra* and/or *XMM-Newton* data (Paper II; this work; Tsujimoto et al. 1999; Sasaki, Pietsch, & Haberl 2003). Moreover, of these six sources, only [NHS03] 70 appear to stay at a stable low luminosity level since 2000 Oct. (Rev. 0157). In addition, all but [NHS03] 4 possess an emission-line, early-type counterpart (see e.g. Paper II). However, we may note that the candidate counterpart of Source V ([MA93] 1277, see Sasaki et al. 2003) lies rather far away (>6″) from the X-ray source, a distance much larger than for the other cases which might cast doubt on the identification.

A few other XRB candidates have recently been proposed by Sasaki, Pietsch, & Haberl (2003): [NHS03] 75, and Sources I & N. The varying character of these sources, confirmed by our new *XMM-Newton* observation, and the presence of a bright blue counterpart left little doubt about their XRB nature. This is especially true for Source I, discovered recently to pulsate in the X-ray domain (Majid, Lamb, & Macomb 2004). In addition, we observe a clear variation of the flux of [NHS03] 69 in the last *XMM-Newton* observation. Since pulses were also detected for this source by Lamb et al. (2002), its identification as an X-ray binary

[4]Note that Macomb et al. (2003) failed to detect the variations of [NHS03] 6 over the *Chandra* exposure, which we reported in Paper II.

is extremely likely.

In Paper II, because of the estimated spectral types of their counterparts or due to their variable nature, we had also tentatively proposed a few new XRB candidates. Of these, [NHS03] 3, 9 and 34 were unfortunately too faint to be detected by *XMM-Newton*, and [NHS03] 61 and 68 do not show any flux variation between the *XMM-Newton* observations. However, [NHS03] 10 and 71 present small variations: these sources should be considered as the best choices for future studies of XRB candidates. Outside *Chandra* FOV, another X-ray source may constitute an additional XRB candidate: Source U. We estimated a B spectral type for its counterpart (see Table 3) but no variations of the X-ray properties of the source were detected between our two *XMM-Newton* observations.

Such a large number of XRBs in the SMC is not at all surprising (e.g. Haberl & Sasaki 2000), but a precise knowledge of their exact number and physical properties may enable us to better constrain their dependence on metallicity. The next step will be to monitor the counterparts of all these sources to find the physical parameters of these systems, and especially to determine the exact nature of the accretor.

Finally, the variability of the other sources described in §3.3 is an interesting new discovery, that can give hints on the exact nature of these sources. They might be additional X-ray binaries, or varying extragalactic sources (AGNs). In this context, we may note that using the formalism of Giacconi et al. (2001), we expect about 20 extragalactic sources in this field. Such sources should be well fitted by power-laws, but should also display a large absorbing column. The large slopes Γ of [NHS03] 24, 46, & 60 and of Sources G & L may indicate that these sources are likely AGNs. Note however that amongst these, only Source G has a very large absorption column. Moreover, the known X-ray binary [NHS03] 4 was also fitted by a power-law of large energy slope Γ, and X-ray binaries containing a black hole can present large Γ in their soft state (e.g. Cyg X-1). Long term monitoring of these sources and a precise study of their actual counterparts are needed, in order to better constrain their nature.

5. Summary and conclusion

In this third Paper on the X-ray emission from the NGC 346 field, we have analyzed *XMM-Newton* data taken six months before and after *Chandra*'s observations. 51 sources were detected with *XMM-Newton*, 29 of them being in common with the *Chandra* data analyzed in Paper II. A comparison of the X-ray observations of the field has revealed the variations of nearly half of the X-ray sources, but only 10 of them were known as X-

ray binaries or XRB candidates. One of these varying sources is HD 5980, which appears brighter during the first *XMM-Newton* observation. However, the exact nature of these changes (secular or phase-locked variations ?) is not yet known, and requests additional X-ray data to be elucidated.

Y.N. acknowledges support from the PRODEX XMM-OM and Integral Projects, contracts P4/05 and P5/36 'Pôle d'Attraction Interuniversitaire (SSTC-Belgium). This Paper utilizes public domain data from the 2MASS, USNO, and the GSC. This research has made use of the SIMBAD database, operated at CDS, Strasbourg, France and NASA's Astrophysics Data System Abstract Service. The authors also acknowledge HEASARC for providing FTOOLS and XSPEC and the referee for useful comments.

REFERENCES

Arnaud, K. 1996, ASP Conf. Ser. 101, eds G. Jacoby & J. Barnes, p.17

Blackburn, J.K. 1995, in ASP Conf. Ser., Vol. 77, Astronomical Data Analysis Software and Systems IV, eds. R.A. Shaw, H.E. Payne, and J.J.E. Hayes (San Francisco: ASP), 367

Giacconi, R., Rosati, P., Tozzi, P., Nonino, M., Hasinger, G., Norman, C., Bergeron, J., Borgani, S., Gilli, R., Gilmozzi, R., & Zheng, W. 2001, ApJ, 551, 624

Claeskens, J.-F., et al. 2004, A&A (submitted)

Haberl, F. 2003, COSPAR Symposium on High Energy Studies of Supernova Remnants and Neutron Stars, Houston, Oct. 2002 (astro-ph/0302540)

Haberl, F., Filipovic, M. D., Pietsch, W., & Kahabka, P. 2000, A&AS, 142, 41 (HFP2000)

Haberl, F., & Sasaki, M. 2000, A&A 359, 573

Haberl, F., & Pietsch, W. 2004, A&A, 414, 667

Kaastra, J.S. 1992, An X-Ray Spectral Code for Optically Thin Plasmas (Internal SRON-Leiden Report, updated version 2.0)

Kahabka, P., Pietsch, W., Filipovic, M.D., & Haberl, F. 1999, A&AS, 136, 81

Jansen, F., Lumb, D., Altieri, B., et al. 2001, A&A, 365, L1

Lamb, R.C., Fox, D.W., Macomb, D.J., & Prince, T.A. 2002, ApJ, 574, L29

Lejeune, T. & Schaerer, D. 2001, A&A, 366, 538

Macomb, D.J., Fox, D.W., Lamb, R.C., & Prince, T.A. 2003, ApJ, 584, L79

Majid, W.A., Lamb, R.C., & Macomb, D.J. 2004, ApJ, submitted (astro-ph/0312034)

Massey, P., Parker, J.W., & Garmany, C.D. 1989, AJ, 98, 1305

Meyssonnier, N., & Azzopardi, M. 1993, A&AS, 102, 451 (MA93)

Nazé Y., Hartwell, J.M., Stevens, I.R., Corcoran, M.F., Chu, Y.-H., Koenigsberger, G., Moffat, A.F.J., & Niemela, V.S. 2002, ApJ, 580, 225 (Paper I)

Nazé Y., Hartwell, J.M., Stevens, I.R., Manfroid, J., Marchenko, S., Corcoran, M.F., Moffat, A.F.J., & Skalkowski, G. 2003, ApJ, 586, 983 (Paper II, sources numbered [NHS03])

Sana, H., Stevens, I.R., Gosset, E., Rauw, G., & Vreux, J.-M. 2004, MNRAS, in press

Sasaki, M., Haberl, F., & Pietsch, W. 2000, A&AS, 147, 75 (SHP2000)

Sasaki, M., Pietsch, W., & Haberl, F. 2003, A&A, 403, 901

Sterken, C. & Breysacher, J. 1997, A&A, 328, 269

Strüder, L., Briel, U., & Dennerl, K. et al. 2001, A&A, 365, L18

Tsujimoto, M., Imanishi, K., Yokogawa, J., & Koyama, K. 1999, PASJ, 51, L21

Turner, M.J.L., Abbey, A., Arnaud, M., et al. 2001, A&A, 365, L27

XMM-Newton Survey Science Centre Consortium 2003, *XMM-Newton* Serendipitous Source Catalogue (1XMM)

Ye, T., Turtle, A.J., & Kennicutt, R.C., Jr. 1991, MNRAS, 249, 722

Yokogawa, J., Imanishi, K., Tsujimoto, M., Nishiuchi, M., Koyama, K., Nagase, F., Corbet, R.H.D. 2000, ApJS, 128, 491 ([YIT2000])

This preprint was prepared with the AAS LaTeX macros v5.2.

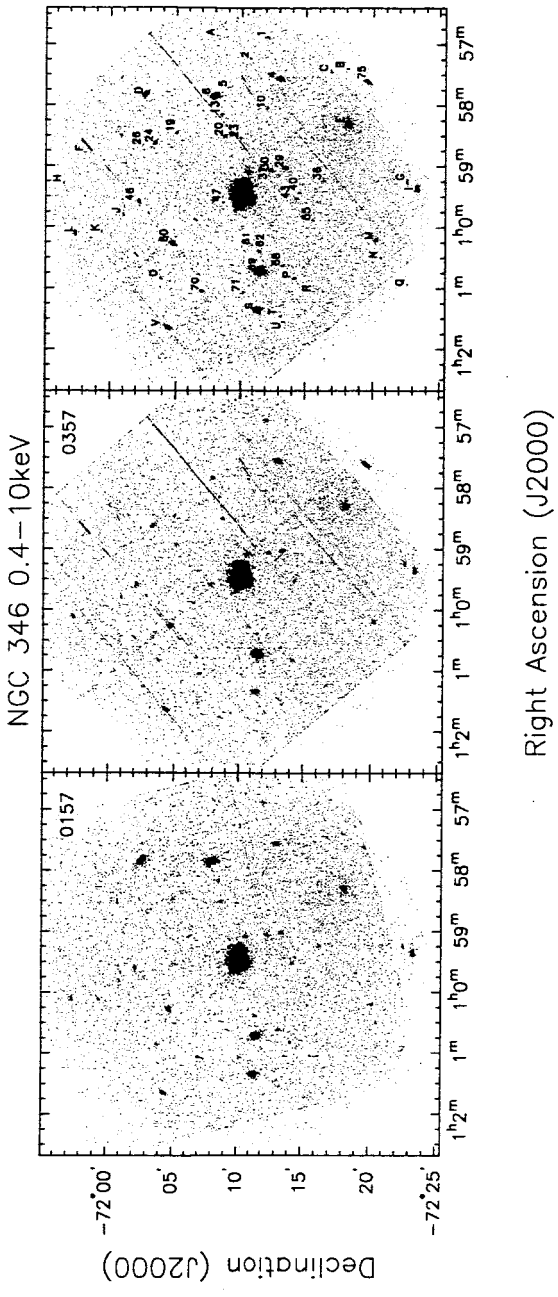

Fig. 1.— The NGC 346 field as seen by the EPIC instruments onboard *XMM-Newton*. Left: data from Rev. 0157, Middle: data from Rev. 0357, Right: combined data from both revolutions with identification numbers (see Table 1 for a precise list of positions). Note that these figures were made by keeping the EPIC pn events with a pattern between 0 and 12 and passing through the #XMMEA_EP filter.

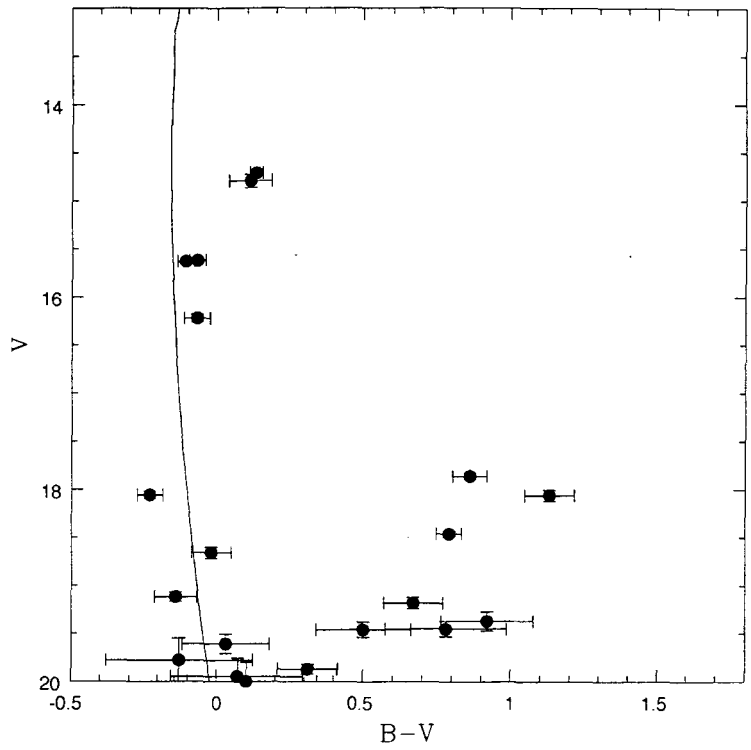

Fig. 2.— The Color-Magnitude Diagram of the counterparts listed in Table 3. The error bars correspond to the dispersion of the measured data. Counterparts with $V > 20$ mag were not included since their photometry is very uncertain. The solid line shows an isochrone of 5 Myr for Z=0.004 (Lejeune & Schaerer 2001) transformed using a distance of 59 kpc and reddened with R_V=3.3 and $E(B-V)$ of 0.14 mag (Massey, Parker & Garmany 1989).

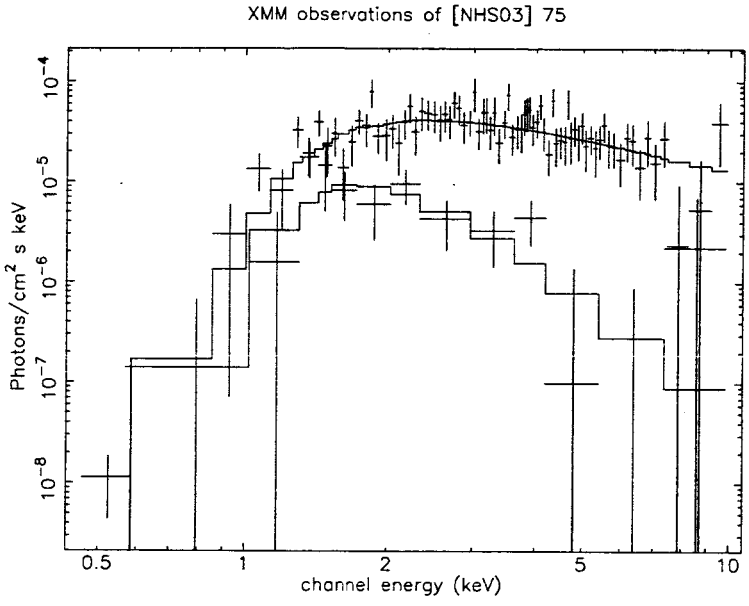

Fig. 3.— Unfolded spectra of [NHS03] 75 in the two *XMM-Newton* observations, shown along with the best fit power law (see Table 2). The upper spectrum presents the EPIC MOS2 data of Rev. 0357, and the lower one corresponds to the EPIC MOS1 data of Rev. 0157 (in the other cameras, the source was either in a gap, out of FOV or close to the edge of the FOV). In Rev. 0157, the luminosity in the 0.4−10 keV energy range has decreased by $> 200\%$, while the power law slope has steepened from 1.1 to 3.9.

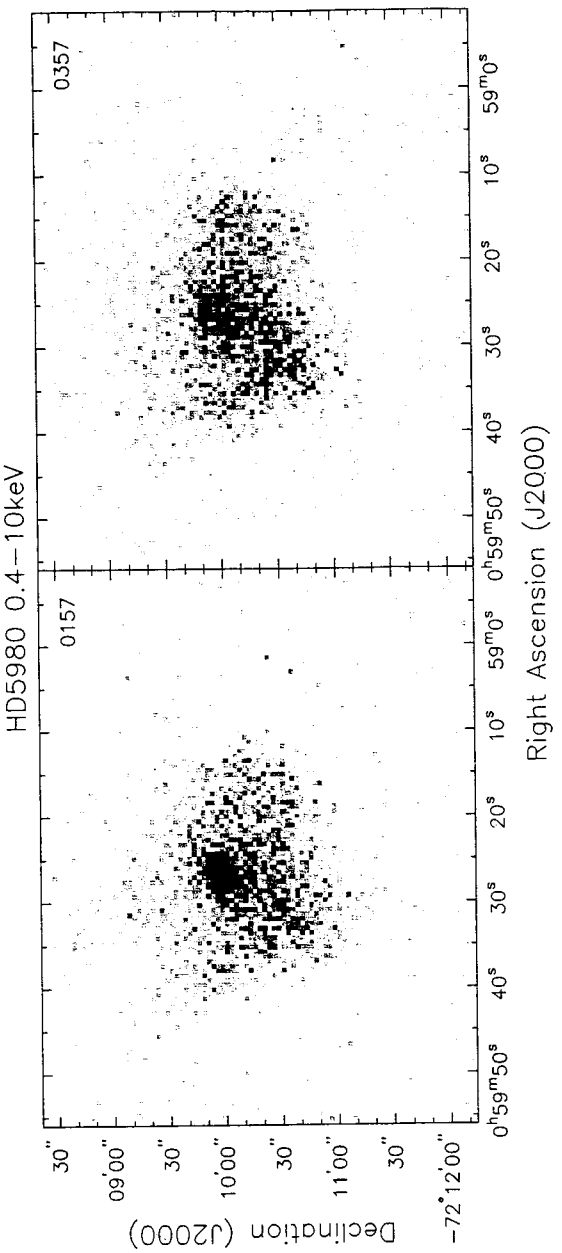

Fig. 4.— EPIC image of the SNR and HD 5980 for both observations. The cluster NGC 346 is just barely visible to the south-west of the SNR, at position $0^h59^m04^s$ $-72°10'35''$(whereas HD 5980 is at $0^h59^m26^s$ $-72°09'53''$). This figure uses the same event lists as Fig. 1.

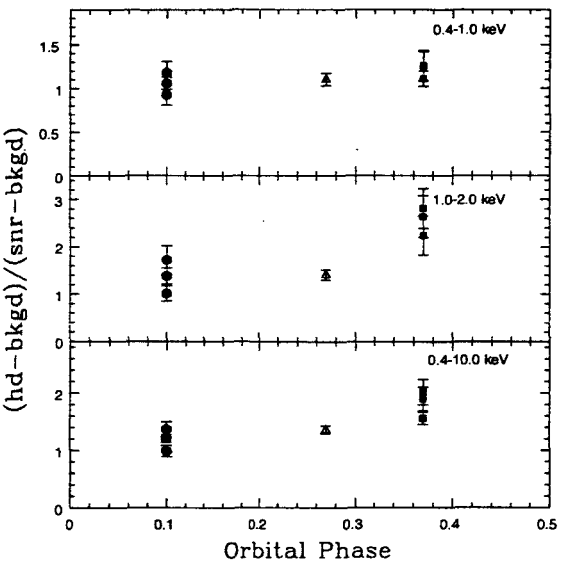

Fig. 5.— Evolution of the diagnostic ratio for HD 5980 (see text): open triangles show the *Chandra* data, filled squares the *XMM-Newton* data from Rev. 0157 and filled circles the *XMM-Newton* data from Rev. 0357. The three points for each *XMM-Newton* observation correspond to the ratio evaluated for the three EPIC cameras. The hard X-ray luminosity of HD 5980 is clearly increasing in the *XMM-Newton* observation from Rev. 0157.

Table 1: Characteristics of the sources detected in the *XMM-Newton* data. The first column gives the source number from Paper II, or a letter for the new sources. The second column gives the variability status of the source: 'Y' for variable sources, 'N' (resp. 'n') if no variability was detected in the *Chandra* and *XMM-Newton* observations (resp. only in the *XMM-Newton* observations), and '?' for an uncertain status. The first column of each revolution yields the name of the source according to the conventions for serendipitous *XMM-Newton* sources. The vignetting and background corrected EPIC-MOS and pn count rates in the 0.4–4.0 keV band are indicated for each instrument in 10^{-3} cts s^{-1}, but the hardness ratios are given only for the pn data. The upper limits were determined using the task *esensmap* (with *mlmin*=10). For sources affected by the gaps between the detectors or that are out of the FOV, we do not quote any count rate for the corresponding instrument. In the last column, we quote the information (nature, name, pulse period) known on the X-ray source and/or its counterpart (Paper II; this work; Haberl & Pietsch 2004; Majid, Lamb, & Macomb 2004; Lamb et al. 2002).

Src	V	?	Rev. 0357					
				MOS1	MOS2	pn	HR1	HR2
1	N		XMMU J005652.2−721203	2.99±0.62	4.21±0.76	13.2±1.6	−0.11±0.14	−0.28±0.16
2	n	?	XMMU J005713.0−721041	1.42±0.49	1.08±0.47	3.89±0.99	−0.26±0.27	−0.11±0.40
4	Y		XMMU J005732.5−721302	18.9±1.2	18.4±1.2	74.0±3.0	−0.14±0.04	−0.44±0.05
75	Y		XMMU J005735.6−721934		68.5±2.6			
5	n	?	XMMU J005741.8−720900	0.81±0.34	0.89±0.39	3.02±0.72	0.82±0.25	−0.34±0.25
6	Y		XMMU J005749.9−720756	2.86±0.52	4.40±0.63	9.11±1.08	0.66±0.14	−0.20±0.12
10	Y		XMMU J005802.5−721205	0.83±0.32	1.54±0.40	1.46±0.63	−0.32±0.50	0.06±0.60
13	n		XMMU J005808.7−720826	1.27±0.37		2.80±0.67	0.45±0.30	−0.16±0.26
19	N		XMMU J005827.3−720500	1.39±0.38	1.82±0.47	2.97±0.62	1.00±0.46	0.22±0.18
20	N		XMMU J005830.1−720842	1.66±0.34	1.53±0.39	5.39±0.73	0.09±0.15	−0.38±0.16
23	Y			<1.0	<1.3			
24	Y		XMMU J005836.8−720326	4.06±0.60	4.15±0.66			
26	n	?	XMMU J005839.7−720229	1.07±0.40	1.21±0.42	3.23±0.77	0.52±0.30	−0.20±0.25
29	N		XMMU J005900.8−721329	3.03±0.42	3.36±0.47			
30	N		XMMU J005903.1−721224	2.55±0.37	4.03±0.49			
36	n		XMMU J005912.9−721620	1.13±0.70	0.25±0.37	4.62±0.81	−0.11±0.17	−0.64±0.27
37	Y		XMMU J005918.0−721112	0.52±0.24	0.55±0.27	3.15±0.68	−0.17±0.25	−0.13±0.26
40	n		XMMU J005925.3−721432	0.66±0.25	0.64±0.26	2.83±0.60	−0.01±0.21	−0.81±0.25
43	n		XMMU J005931.6−721417	0.72±0.25	1.08±0.32	1.76±0.51	1.00±1.37	0.54±0.26
46	Y		XMMU J005935.0−720211	4.68±0.67	4.48±0.61			
47	Y		XMMU J005935.4−720836	0.52±0.25	0.20±0.23	2.25±0.50	0.83±0.35	0.07±0.21
55	n	?		<1.1	<1.4	<2.0		
60	Y		XMMU J010015.5−720442	9.36±0.85	12.3±1.0			
61	Y		XMMU J010017.2−721054	0.49±0.26	1.47±0.39			
62	n		XMMU J010022.9−721130	1.01±0.34	1.62±0.39	4.02±0.70	−0.20±0.17	−0.71±0.29
68	n		XMMU J010037.8−721314	0.77±0.30	1.66±0.44	1.30±0.53	1.00±0.86	0.22±0.37
69	Y		XMMU J010042.9−721133			227.±4.	0.05±0.02	−0.61±0.02
70	N[a]		XMMU J010102.5−720659	2.29±0.51	4.58±0.68	6.19±0.88	−0.05±0.16	−0.12±0.18
71	Y		XMMU J010103.8−721007	1.33±0.43		3.51±0.75	−0.38±0.22	−0.10±0.34
A	n	?	XMMU J005651.3−720804	2.15±0.63	1.64±0.62	3.66±1.11	1.00±0.37	−0.04±0.29
B	n	?		<1.7	<2.1			
C	n		XMMU J005725.6−721646	1.38±0.49	1.78±0.54	3.72±1.04	0.50±0.28	−0.81±0.26
D	Y			<1.8	<2.0	<2.9		
E	n		XMMU J005816.7−721806	15.8±1.1	17.9±1.2	50.2±2.5	0.23±0.05	−0.45±0.05
F	n	?	XMMU J005846.1−715809	1.60±0.63	0.94±0.51	4.60±1.24	−0.31±0.30	−0.02±0.43
G	Y		XMMU J005914.4−722231	5.58±0.84	6.55±0.92	11.2±1.6	0.59±0.18	−0.03±0.15
H	n	?	XMMU J005916.5−715630	2.84±0.84	2.63±0.79	4.79±1.32	0.00±0.40	0.28±0.31
I	Y		XMMU J005921.0−722317	29.5±1.8	40.3±2.1			
J	n		XMMU J005947.1−720059	1.23±0.46	2.55±0.63	6.61±0.99	0.37±0.17	−0.39±0.16
K	n		XMMU J010004.6−715921	1.29±0.58	0.25±0.39	4.70±1.03	−0.19±0.22	−0.26±0.35
L	Y		XMMU J010005.9−715724	13.7±1.6		30.2±2.5	−0.10±0.09	−0.55±0.11
M	Y		XMMU J010011.8−722013		6.48±0.90	19.8±1.8	0.58±0.09	−0.45±0.09
N	Y			<1.8	<2.1	<3.2		
O	n		XMMU J010049.2−720347	1.91±0.54	3.51±0.65	5.59±0.97	0.68±0.27	0.01±0.17
P	n		XMMU J010049.6−721408	2.75±0.51	2.14±0.52	4.15±0.79	−0.05±0.20	−0.39±0.25
Q	?							
R	n		XMMU J010103.2−721534	0.92±0.37	1.53±0.51	2.27±0.72	0.77±0.46	0.05±0.31
S	Y		XMMU J010120.4−721119	17.5±1.2	26.8±1.6	50.0±2.3	0.39±0.06	−0.07±0.05
T	n		XMMU J010127.4−721305	1.78±0.48	1.60±0.57	2.04±0.85	−0.04±0.48	−0.00±0.53
U	n		XMMU J010133.1−721320	1.34±0.48	2.24±0.59	4.42±0.91	0.03±0.27	0.04±0.24
V	Y		XMMU J010137.4−720420	14.3±1.3	19.3±1.6			

Table 1: Continued

Src	V ?		Rev. 0157 MOS1	MOS2	pn	HR1	HR2	Remarks
1	N	XMMU J005652.3−721206	3.38±0.74	3.04±0.68	7.95±1.50	−0.01±0.20	−0.25±0.26	
2	n?		<2.0	<2.0	<3.5			
4	Y	XMMU J005732.6−721304	12.9±1.2	9.95±1.05	41.8±2.8	−0.09±0.07	−0.47±0.08	XRB cand.
75	Y	XMMU J005736.5−721936	4.30±0.75		15.0±2.1	0.66±0.16	−0.24±0.14	XRB, P=565 s, [MA93]1020
5	n?		<1.7	<1.7	<3.1			
6	Y	XMMU J005750.3−720758	51.4±2.3		120.±4.	0.51±0.04	0.09±0.04	XRB, P=152.3 s, [MA93]1038
10	Y	XMMU J005802.7−721206	1.35±0.40	0.94±0.38	3.02±0.79	0.83±0.33	−0.00±0.26	B star
13	n	XMMU J005809.2−720826	0.90±0.42	0.44±0.36	3.07±0.89	−0.12±0.31	−0.22±0.43	
19	N	XMMU J005828.0−720501	1.64±0.48		4.10±0.77	0.96±0.14	−0.22±0.19	
20	N	XMMU J005830.1−720844	2.17±0.42	1.78±0.42	5.78±0.88	0.45±0.19	−0.19±0.16	
23	Y	XMMU J005831.7−720953	0.85±0.33	0.73±0.27	1.81±0.61	0.73±0.52	0.19±0.33	
24	Y	XMMU J005838.1−720324			3.35±0.87	0.61±0.22	−1.00±0.36	
26	n?		<2.1					
29	N	XMMU J005901.1−721331	2.95±0.45	4.17±0.53	6.36±0.94	1.00±0.18	−0.11±0.14	A star
30	N	XMMU J005903.3−721226	2.72±0.40	3.15±0.49				
36	n	XMMU J005913.4−721620	1.55±0.39	1.04±0.34				
37	Y		<1.3	<1.2	<2.6			
40	n	XMMU J005925.8−721433	0.61±0.26	0.23±0.23	2.07±0.57	1.00±0.22	−0.59±0.30	
43	n	XMMU J005931.5−721419	0.73±0.27	1.16±0.30				
46	Y	XMMU J005934.9−720213	5.03±0.81	3.13±0.64	8.84±1.26	−0.05±0.15	−0.46±0.18	
47	Y	XMMU J005935.2−720837	0.38±0.27	0.98±0.28	0.86±0.44	1.00±0.31	−0.53±0.48	
55	n?	XMMU J005952.8−721533	0.61±0.31	0.84±0.33	1.88±0.68	0.34±0.58	0.19±0.36	
60	Y	XMMU J010015.7−720444	8.17±0.93	7.78±0.90	20.7±1.6	0.32±0.08	−0.46±0.08	XRB cand. or AGN ?
61	Y	XMMU J010017.3−721051	0.86±0.33	0.71±0.34	1.27±0.60	1.00±1.05	0.27±0.44	B star
62	n	XMMU J010023.3−721131	1.65±0.45	1.44±0.39	6.08±0.96	−0.41±0.15	−0.52±0.31	
68	n	XMMU J010036.7−721321	1.11±0.38	0.85±0.37	1.81±0.72	−1.00±15.7	1.00±0.43	B star
69	Y	XMMU J010043.0−721135	68.0±2.4		200.±5.	0.05±0.03	−0.63±0.03	XRB, P=5.44 s, B star
70	N[a]	XMMU J010103.1−720702	3.42±0.60	4.34±0.64	8.90±1.18	−0.05±0.15	−0.16±0.17	XRB, P=304.5 s, [MA93]1240
71	Y	XMMU J010103.8−721007	1.32±0.47	1.94±0.55				B star
A	n?		<2.6	<2.5	<4.3			
B	n?	XMMU J005722.8−721759	1.36±0.60	1.53±0.59	5.45±1.26	0.91±0.25	−0.22±0.23	
C	n	XMMU J005726.5−721649	1.53±0.52	1.64±0.60	3.85±1.31	−0.14±0.37	−0.17±0.45	
D	Y	XMMU J005749.7−720238	49.6±2.9	39.4±2.2	86.2±3.8	0.19±0.05	−0.08±0.05	XRB, P=280.4 s, [MA93]1036
E	n	XMMU J005816.8−721806	14.8±1.3	12.7±1.2	48.4±3.0	0.19±0.07	−0.17±0.07	SNR 0056−72.5
F	n?		<2.8					
G	Y	XMMU J005914.2−722232	5.99±0.96	5.48±0.93				
H	n?				<4.6			
I	Y	XMMU J005921.0−722318	44.1±2.4	48.0±2.6				XRB, P=202 s
J	n	XMMU J005947.0−720057	2.58±0.71	2.53±0.69				
K	n	XMMU J010005.1−715925	0.96±0.64	1.18±0.65				
L	Y	XMMU J010005.8−715725		6.50±1.34	19.5±2.4	0.02±0.13	−0.48±0.15	
M	Y	XMMU J010012.0−722014	3.79±0.75		10.5±1.5	0.27±0.18	−0.07±0.16	
N	Y	XMMU J010030.2−722033	2.52±0.62	2.18±0.67	8.84±1.58	0.82±0.19	−0.25±0.17	XRB cand., [MA93]1208
O	n	XMMU J010049.9−720351	2.55±0.58	4.04±0.70	5.02±1.06	0.62±0.23	−0.41±0.22	
P	n	XMMU J010049.8−721410	1.56±0.45	3.38±0.59				
Q	?	XMMU J010057.4−722231	4.19±0.89	6.15±1.06				
R	n	XMMU J010103.2−721538	0.75±0.38	1.00±0.46	2.78±0.88	0.67±0.35	−0.72±0.30	
S	Y	XMMU J010120.7−721120	32.5±1.9	32.5±2.0	83.3±3.6	0.24±0.05	0.06±0.05	XRB, P=455 s, [MA93]1257
T	n	XMMU J010127.9−721305	0.53±0.41	1.26±0.51	5.94±1.24	−0.13±0.22	−0.37±0.32	
U	n	XMMU J010133.2−721322	2.06±0.60	1.53±0.56	3.91±1.14	0.46±0.37	−0.22±0.30	B star
V	Y	XMMU J010137.6−720421	10.1±1.2	10.7±1.2	34.2±2.5	0.10±0.08	−0.26±0.09	XRB cand., [MA93]1277

[a]This source did not vary between our three datasets, but was observed by *ROSAT* to be much brighter (see Paper II).

Table 2: Parameters of the spectral fits. Γ is the photon index of the power law, and the quoted limits correspond to the 90% confidence interval. Abundances are fixed at $0.1Z_{\odot}$, except for [NHS03] 69 for which it was fitted ($Z_{0157} = 0.0015^{0.0039}_{0.0001}$ and $Z_{0357} = 0.0003^{0.0014}_{0.0001}$, to be compared with $Z_{Ch} = 0.0022^{0.0094}_{0.0001}$, cfr. Paper II). Absorbed luminosities in the spectral range 0.4−10 keV are given for a distance of 59 kpc, and clearly unphysical models have been discarded. All available EPIC spectra were fitted simultaneously. For comparison, the 90% confidence intervals and the luminosity of the *Chandra* data are presented in the last columns.

Src	*XMM-Newton* Rev. 0157				*XMM-Newton* Rev. 0357				Chandra		
	N(H) (10^{22} cm^{-2})	(kT in keV)	χ^2_ν(dof)	L_X^{abs} (10^{34} ergs s^{-1})	N(H) (10^{22} cm^{-2})	(kT in keV)	χ^2_ν(dof)	L_X^{abs} (10^{34} ergs s^{-1})	N(H) (10^{22} cm^{-2})	(kT in keV)	L_X^{abs} (10^{34} ergs s^{-1})
[NHS03] 4 mek.	$0.^{0.04}_{0.}$	kT=$3.01^{4.48}_{2.13}$	1.12 (73)	3.68	$0.05^{0.07}_{0.02}$	kT=$2.27^{2.83}_{1.96}$	1.04 (161)	6.50	0.13−0.19	kT=2.5−3.6	4.21
[NHS03] 4 pow.	$0.08^{0.17}_{0.01}$	$\Gamma = 2.20^{2.62}_{1.97}$	1.11 (73)	3.97	$0.21^{0.26}_{0.15}$	$\Gamma = 2.66^{2.89}_{2.37}$	0.99 (161)	6.71	0.24−0.32	Γ=2.2−2.5	4.54
[NHS03] 6 pow.	$0.31^{0.39}_{0.25}$	$\Gamma = 0.81^{0.89}_{0.76}$	0.94 (309)	60.0	$0.49^{1.01}_{0.25}$	$\Gamma = 1.53^{1.90}_{1.05}$	1.00 (67)	2.54	0.45−0.56	Γ=0.80−0.93	55.4
[NHS03] 60 mek.	$0.04^{0.21}_{0.}$	kT=$5.66^{43.}_{2.37}$	1.15 (26)	4.00	$0.06^{0.16}_{0.}$	kT=$4.08^{13.}_{2.21}$	1.42 (46)	4.00	0.33−0.58	kT=2.46−8.63	1.15
[NHS03] 60 pow.	$0.12^{0.34}_{0.}$	$\Gamma = 1.82^{2.57}_{1.29}$	1.15 (26)	4.29	$0.18^{0.35}_{0.05}$	$\Gamma = 2.17^{2.83}_{1.76}$	1.35 (46)	4.05	0.35−0.77	Γ=1.71−2.46	1.27
[NHS03] 69 mek.	$0.23^{0.26}_{0.20}$	kT=$0.98^{1.10}_{0.90}$	0.95 (241)	15.1	$0.20^{0.23}_{0.17}$	kT=$1.17^{1.30}_{1.04}$	0.74 (253)	18.0	0.38−0.44	kT=0.99−1.11	14.8
[NHS03] 69 pow.	$0.44^{0.48}_{0.40}$	$\Gamma = 3.62^{3.81}_{3.45}$	1.06 (242)	15.7	$0.39^{0.43}_{0.36}$	$\Gamma = 3.34^{3.52}_{3.17}$	0.76 (254)	19.1	0.67−0.75	Γ=3.71−3.93	13.5
[NHS03] 75 pow.	$2.61^{5.23}_{0.84}$	$\Gamma = 3.90^{6.39}_{1.85}$	0.80 (10)	2.95	$1.73^{2.44}_{1.21}$	$\Gamma = 1.14^{1.51}_{0.83}$	0.86 (75)	69.3			
D pow.	$0.05^{0.21}_{0.}$	$\Gamma = 0.79^{1.03}_{0.57}$	0.78 (46)	44.1							
E pow.	$0.17^{0.26}_{0.10}$	$\Gamma = 1.53^{1.75}_{1.35}$	0.95 (105)	9.26	$0.19^{0.26}_{0.09}$	$\Gamma = 1.81^{2.12}_{1.55}$	0.86 (70)	9.07			
G pow.	$1.54^{3.11}_{0.60}$	$\Gamma = 2.70^{4.59}_{1.55}$	1.07 (13)	3.41	$0.95^{1.99}_{0.31}$	$\Gamma = 2.32^{3.88}_{1.28}$	1.42 (20)	2.94			
I pow.	$0.18^{0.30}_{0.09}$	$\Gamma = 1.28^{1.48}_{1.09}$	0.71 (75)	34.4	$0.37^{0.52}_{0.25}$	$\Gamma = 1.49^{1.75}_{1.26}$	0.99 (68)	21.0			
L mek.	$0.06^{0.16}_{0.}$	kT=$1.96^{5.22}_{1.31}$	1.06 (36)	1.87	$0.07^{0.17}_{0.}$	kT=$3.09^{13.}_{1.63}$	1.11 (51)	3.22			
L pow.	$0.23^{0.43}_{0.09}$	$\Gamma = 2.84^{4.53}_{1.94}$	1.05 (36)	1.91	$0.18^{0.27}_{0.05}$	Γ=$2.24^{3.14}_{1.88}$	1.09 (51)	3.47			
S pow.	$0.11^{0.20}_{0.04}$	$\Gamma = 0.60^{0.71}_{0.50}$	1.23 (194)	38.3	$0.18^{0.29}_{0.10}$	$\Gamma = 0.90^{1.05}_{0.79}$	0.99 (172)	18.8			
V pow.	$0.20^{0.38}_{0.05}$	$\Gamma = 2.10^{2.77}_{1.72}$	0.93 (58)	4.02	$0.09^{0.25}_{0.}$	$\Gamma = 1.67^{2.07}_{1.25}$	1.19 (40)	7.81			

Table 3: Counterparts of the X-ray sources. The second column gives the *ROSAT* or *ASCA* name of the source (y=[YIT2000], h=[HFP2000], s=[SHP2000]), while the following columns present the WFI photometry of the optical counterparts, with the separation between the X-ray sources and their counterparts. The error quoted in the σ_V column represents the dispersion of the measured data. If the counterpart is cataloged, the identifier, starting by S for GSC 2.2, U for USNO-B1.0, or 2M for 2MASS all Sky Survey, is given in the last column of the Table. When it was possible, an estimation of the spectral type of the counterpart was made (in italics, see last column), assuming that it belongs to NGC 346 ($E(B-V)$=0.14 mag, d=59 kpc).

Src	*ROSAT* or *ASCA*	V (mag)	$B-V$ (mag)	$U-B$ (mag)	$V-R$ (mag)	$R-I$ (mag)	σ_V (mag)	d157 (″)	d357 (″)	Remarks
A		17.86	0.86	1.06	0.50	0.48	0.03		2.3	U0178-0040763 =2M00565129−7208034
B		18.46	0.79	0.15	0.45	0.34	0.03	3.8		S01020202023
C		20.30	−0.30		0.45		0.20	1.3	3.5	
		19.61	0.03		−0.01		0.10	3.2	3.9	*B9V?*
D	y20,h114	15.62	−0.07	−0.96	0.09	−0.02	0.02	1.2		*lateO, earlyBV*,[MA93]1036[a]
E	y21,h194	20.00	0.10		−0.08		0.20	3.3	4.7	SNR 0056−72.5
F		18.06	−0.23	−0.76	−0.10	−0.05	0.04		4.0	
G	s80	19.37	0.92	−0.77	0.59	0.79	0.10	0.5	2.4	
H		19.78	−0.13	−0.31	0.05	0.55	0.23		3.0	
I	h218	14.79	0.11	−1.09	−0.02	−0.05	0.07	0.6	2.2	S010231088040=U0176-0044581 =2M00592103−7223173
J	y23,h102	19.45	0.78		0.48	0.66	0.08	2.0	2.3	
K		19.87	0.31		0.34	0.28	0.05	2.0	1.7	
		19.46	0.50		0.39	0.25	0.08	2.4	4.0	
L	h91	19.18	0.67	−0.47	0.19	0.63	0.06	0.6	2.5	
M	h204									
N		14.71	0.13	−1.06	0.10	0.01	0.02	2.0		[MA93]1208[b]
O	s91	19.12	−0.14	−0.54	−0.18		0.05	5.0	3.0	
P	h177	19.95	0.07	−0.36	−0.39		0.19	3.2	3.5	
Q	h213	18.06	1.13	0.26	0.53	0.54	0.06	3.5		U0176-0047908
S	h159	15.63	−0.11	−1.06	0.02	−0.03	0.02	0.7	1.2	*lateO, earlyBV*,[MA93]1257[c]
T	y27	21.26	−0.17		−0.12	2.84	0.27	3.0	3.0	
U		18.66	−0.02	−0.48	−0.03	0.09	0.06	3.9	3.5	*B5 − 7V*
V	h121	16.22	−0.07	−0.90	0.05	−0.02	0.04	5.7	7.7	*B1V*,[MA93]1277[d]

[a]=S010202024704=U0179-0037591=2M00574957−7202361

[b]=S010231095307=U0176-0047027=2M01003000−7220335

[c]=S010202097167=0178-0047126=2M01012065−7211192

[d]=S010202021404=U0179-0043444=2M01013695−7204148, 6−8″distant but considered as the counterpart by Haberl & Sasaki (2000); Sasaki, Pietsch, & Haberl (2003).